Nanoscale

PAPER

View Article Online
View Journal

Cite this: DOI: 10.1039/d2nr01132h

3d transition metal coordination on monolayer MoS_2: a facile doping method to functionalize surfaces†

He Liu,‡[a] Walner Costa Silva,‡[b] Leonardo Santana Gonçalves de Souza,[b] Amanda Garcez Veiga,[b] Leandro Seixas,[c,d] Kazunori Fujisawa,[e,f,g] Ethan Kahn,[h] Tianyi Zhang,[h] Fu Zhang,[h] Zhuohang Yu,[h] Katherine Thompson,[a] Yu Lei,[h] Christiano J. S. de Matos,[c,d] Maria Luiza M. Rocco,[b] Mauricio Terrones *[a,f,g,h] and Daniel Grasseschi *[b]

Two-dimensional materials (2DM) have attracted much interest due to their distinct optical, electronic, and catalytic properties. These properties can be tuned by a range of methods including substitutional doping and, as recently demonstrated, by surface functionalization with single atoms, thus increasing the 2DM portfolio. We theoretically and experimentally describe the coordination reaction between MoS_2 monolayers and 3d transition metals (TMs), exploring their nature and MoS_2–TM interactions. Density functional theory calculations, X-ray photoelectron spectroscopy (XPS), and photoluminescence (PL) spectroscopy point to the formation of MoS_2–TM coordination complexes, where the adsorption energy for 3d TMs resembles the crystal-field (CF) stabilization energy for weak-field complexes. Pearson's theory for hard–soft acid–base and ligand-field theory were used to discuss the periodic trends of 3d TM coordination on MoS_2 monolayer surfaces. We found that softer acids with higher ligand field stabilization energy, such as Ni^{2+}, tend to form bonds with more covalent character with MoS_2, which can be considered a soft base. On the other hand, harder acids, such as Cr^{3+}, tend to form more ionic bonds. Additionally, we studied the trends in charge transfer and doping observed from XPS and PL results, where metals like Ni led to n-type doping. In contrast, Cu functionalization results in p-type doping. Therefore, the formation of coordination complexes on TMD's surface is a potentially effective way to control and understand the nature of single-atom functionalization of TMD monolayers without relying on or creating new defects.

Received 28th February 2022,
Accepted 10th June 2022

DOI: 10.1039/d2nr01132h

rsc.li/nanoscale

Introduction

In 2D materials (2DM), functionalization and doping are commonly accomplished through the induction of vacancies within the crystalline lattice or through the formation of substitutional sites, where atoms with a greater or lesser number of electrons are placed as dopants for the creation of semiconductors of type n or p, or through the formation of covalent bonds between organic molecules and atoms at the edges of the materials.[1–4] However, these interactions can be unstable and/or significantly alter the crystalline structure of 2D materials, thus modifying their intrinsic properties and stability. It was recently proposed that the physical adsorption of organic molecules or metallic atoms as a functionalization method can be an effective and damage-free way of altering the properties of 2D materials.[5–7]

Lei *et al.* showed theoretically and experimentally that the presence of nonbonding electron pairs on the surface of InSe could be exploited by applying Lewis acid–base concepts.[8] Thus, simple acid–base reactions could be explored to form

[a]*Department of Chemistry, The Pennsylvania State University, University Park, PA, 16802, USA. E-mail: mut11@psu.edu*
[b]*Institute of Chemistry, Federal University of Rio de Janeiro (UFRJ), 21941-909 Rio de Janeiro, Brazil. E-mail: dgrasseschi@iq.ufrj.br*
[c]*MackGraphe-Graphene and Nanomaterials Research Center, Mackenzie Presbyterian Institute, 01302-907 São Paulo, Brazil*
[d]*Engineering School, Mackenzie Presbyterian University, 01302-907 São Paulo, Brazil*
[e]*Research Initiative for Supra-Materials (RISM), Shinshu University, 4-17-1 Wakasato, Nagano, 380-8553, Japan*
[f]*Department of Physics, The Pennsylvania State University, University Park, PA, 16802, USA*
[g]*Center for 2-Dimensional and Layered Materials, The Pennsylvania State University, University Park, PA, 16802, USA*
[h]*Department of Materials Science and Engineering, The Pennsylvania State University, University Park, PA, 16802, USA*
†Electronic supplementary information (ESI) available. See DOI: **https://doi.org/10.1039/d2nr01132h**
‡Equal contributors.

complexes between Lewis acids, such as Ti^{4+}, and 2D materials. Depending on the strength of the acid, it is possible to control the material's Fermi level and bandgap.[8] This opens a vast range of potential applications for these materials to fabricate photovoltaic devices. In this context, Ding *et al.* showed by density functional theory (DFT) that the adsorption of 3d transition metal (TM) atoms on the phosphorene surface is favorable, except for Zn.[9] Similarly, Hashmi *et al.* showed by DFT that transition metals coordinate at a "triangular" site on the surface of phosphorene, and the geometry resembles that of an octahedral coordination complex.[10] This concept can be expanded to other 2D materials, such as graphene and transition metal dichalcogenides (TMDs).[11]

Recently, Gangwar *et al.* studied *via* DFT the interactions of first row Single Atom of Transition Metal (SA-TM) with MoS_2.[12] They found that hollow sites (*i.e.*, the position at the center of the hexagons) and Mo sites had very close adsorption energies, both being higher than those for S sites. The trend observed follows the energy stabilization profile of the crystal field (CF) for high-spin complexes, which should explain why the interaction with Zn is not favorable. These authors predicted that there is some coexistence of ionic and covalent bonding between the TM and MoS_2.[12] In this context, Hai *et al.* described theoretically and experimentally how the TM functionalization of MoS_2 could affect the oxygen evolution reaction (OER) on its surface. The MoS_2–TM complexes were synthesized by hydrothermal treatment, and the results showed a monoatomic dispersion functionalization. They found a relationship between TM–S and TM–O bond orders with the OER activity.[13] Liu *et al.* developed a MoS_2–Co catalyst for hydrodeoxygenation. The catalyst was made by hydrothermal treatment, and the Co atoms were dispersed atomically and occupied the Mo, hollow, and S vacancy sites randomly.[14]

Although all these works successfully described the formation of MoS_2–TM complexes, the fundamentals of SA-TM TMD doping and the effects of the TM coordination sphere on the doping level are still missing. Furthermore, a more controllable functionalization with TM is still needed.[15] We recently showed that isolated Au atoms on the MoS_2 surface cause electrons to flow out of the 2D material, increasing the hole concentration on MoS_2.[16] DFT theoretical results revealed that changes in the TM coordination sphere could adjust the MoS_2–TM binding energy. For example, the energy of the MoS_2–Au bond is twice as high when one coordination site on the Au atom is filled by one S atom on the surface of MoS_2 and the other three by Cl anions than when no Cl is present. When Cl anions are present, the electron transfer from MoS_2 to Au is more efficient, leading to more effective p-type doping and better performance in field-effect transistors. Additionally, the electronic band dispersion of MoS_2–Au is drastically affected by the number of Cl atoms on the Au coordination sphere.[16]

Here, we expanded this vision to evaluate the functionalization of the MoS_2 monolayer with several 3d transition metal ions (Cr, Mn, Co, Ni, Cu, and Zn). We focus on the MoS_2–TM interaction to evaluate the formation of coordination complexes on the surface and correlate their properties with classical coordination complexes, thus facilitating functionalization and controlling its optical and chemical properties with minimal damage to the crystalline monolayer. First, the coordination of 3d TM was evaluated by DFT, considering the interaction between MoS_2 and single TM or TM–Cl_3 species. The theoretical calculations were confirmed by X-ray photoelectron spectroscopy (XPS), photoluminescence (PL) spectroscopy, and reflection electron energy loss spectroscopy (REELS). Additionally, the samples were characterized by optical, atomic force, scanning electron, and high-resolution transmission electron microscopy, which confirmed the monolayer nature of MoS_2 and the single atom nature of the functionalization with metals such as Ni. Finally, all observed trends are rationalized in terms of crystal-field stabilization energy, the absolute hardness of the 3d TM, and their reduction standard potentials with respect to the MoS_2 conduction and valence bands.

Methods

The synthesis of monolayer MoS_2 was carried out by a salt-assisted CVD method. A detailed description can be found in our previous publication.[16] The flakes were transferred to a pristine Si/SiO_2 substrate to remove the excess Na salt and MoO_3 used in the growth process.

Functionalization of MoS_2

The MoS_2–TM complex formation was performed by dipping the Si/SiO_2 substrate with the CVD MoS_2 into an ethanol solution of chromium acetate ($Cr_2(CH_3CO_2)_4(H_2O)_2$), manganese acetate ($Mn(CH_3COO)_2$), iron(III) chloride ($FeCl_3$), cobalt chloride ($CoCl_2$), nickel chloride ($NiCl_2$), copper sulfate ($CuSO_4$), or zinc chloride ($ZnCl_2$) with concentrations between 1×10^{-3} and 1×10^{-9} mol L^{-1} for 10 min. The functionalized MoS_2–TM sample was then immersed in isopropanol (IPA) for a few seconds to remove excess of transition metal salts, followed by N_2 drying. Finally, the sample was kept in a vacuum for 10 min before the measurements. Pristine samples were also washed with ethanol and IPA, dried with N_2, and kept in a vacuum for 10 minutes to exclude the effect of ethanol or IPA adsorption on the flake surface.

Raman and photoluminescence (PL) spectroscopy were performed by excitation at 488 nm in a microscope-based Renishaw InVia spectrometer with thermoelectric CCD. For samples of each different transition metal concentration, we characterized approximately the same region of the same flake before and after functionalization. At least five different flakes were measured for each MoS_2–TM complex and TM concentration. PL mappings were obtained using an Alpha 300R Witec confocal Raman microscope with a highly sensitive EMS detector at 488 nm excitation wavelength and 2 mW laser power.

XPS and REELS measurements were conducted in a high-resolution Thermo Scientific ESCALAB 250Xi spectrometer

equipped with an electron energy hemispherical analyzer and using monochromatized Al Kα line (1486.6 eV) excitation. The spectra were energy referenced to the C 1s signal of aliphatic C atoms at the binding energy of 284.8 eV. XPS spectra were collected using X-ray beam spot size = 650 μm with an emission angle of 90° with respect to the sample surface. High-resolution spectra were acquired with 25 eV pass energy. REELS spectra were acquired with the electron source operating at 1 keV.

The computational approach to study the equilibrium structure, stability, and electronic structure of transition metal-doped MoS_2 is based on the SIESTA package's DFT. We used DZP localized basis, norm-conserved pseudopotentials with Troullier–Martins parametrization, mesh cutoff energy of 350 Ry, and k points sampling of Brillouin zone in Monkhorst–Pack algorithm with 10 × 10 × 1 grid. The exchange–correlation functional used is based on PBE generalized-gradient approximation. The calculations were performed within a supercell framework with 3 × 3 unit cells and considering a 8.3% degree of functionalization. All calculations were done considering T = 0 K, and the Fermi level was determined by the average energy of the highest occupied level at the valence band and the lowest unoccupied level. The optimized structure was used for the STEM image simulation using the Prismatic Software.[17] Simulation parameters such as acceleration voltage, spherical aberration (C_3 and C_5), convergence angle, and inner/outer angle for the HAADF detector were set according to experimental conditions.

Microscopy imaging

Aberration corrected high-resolution scanning transmission electron microscopy (AC-HRSTEM) was carried out in an FEI Titan^3 G2 60/300 operated at 80 kV to reduce irradiation damage. A high-angle annular dark-field (HAADF) detector collected the annular dark-field (ADF) signal. A Gaussian blur filter was applied using the ImageJ software to reduce the noise and enhance the visibility of the detailed structure. Raw images were used for acquiring the line profile of the ADF intensity. It is worth noting that prior to the STEM imaging, the CVD-grown MoS_2 was transferred to a TEM grid and then functionalized with 1×10^{-6} mol L^{-1} TM precursor in ethanol solution. Scanning electron microscopy (SEM) was carried out on a PhenomProX (ThermoFisher, Waltham, EUA), operated at 15 kV with a backscattered electron detector. Atomic force microscopy (AFM) images were recorded on a Bruker ICON system in the taping mode using a RTESPA-300 tip.

Results

Prediction of MoS_2–TM complexes *via* DFT

First, a screening simulation was carried out to evaluate the general trend of coordination of different transition metals on the MoS_2 surface and correlate these trends with the classical coordination chemistry theory to rationalize the properties of chemically functionalized MoS_2–TM complexes. Fig. 1a–c show the optimized structures for the semiconductor 1H phase of MoS_2 and the coordination of Co on two different coordination sites on the MoS_2 monolayer. There are three available coordination sites, which we name the H, M, and S sites (Fig. 1a). In the M site, the coordinated metal is located on top of one Mo atom and bound to 3 S atoms, as shown in Fig. 1b. In site H, the TM is located over the center of the MoS_2 hexagonal structure and bound to 3 S atoms, as shown in Fig. 1c. When the metal is coordinated with the S site, it is located directly on top of one sulfur atom and bound just to that atom, similar to the Au atoms reported in a previous work from our group.[16] As discussed in that work,[16] the TM coordination sphere significantly impacts their properties when bound to the MoS_2 surface. Thus, we considered two different cases in all calculations. In the first one, the TM is bound to the MoS_2 as a single adatom, named here MoS_2–TM. For the other case, the TM's coordination sphere was completed by Cl atoms forming an octahedral structure around the TM, where it is bound to three S and three Cl atoms, labeled MoS_2–TM–Cl_3.

Fig. 1d shows the adsorption energy, E_{ads}, modulus as a function of the number of electrons in the 3d orbitals. E_{ads} is defined as: $E_{ads} = E_{MoS_2\text{–}TM} - (E_{TM} + E_{MoS_2})$, where $E_{MoS_2\text{–}TM}$ is the energy of the final MoS_2–TM complex, and $E_{TM} + E_{MoS_2}$ is the sum of the energies of the isolated TM and MoS_2, respectively (Table S1†). A clear trend resembles the one observed for the crystal field stabilization energy and the hydration enthalpy for weak field 3d TM complexes.[18,19] The closed shell (d^{10}) and the half shell (d^5) cases exhibit the lowest adsorption energies due to the spherical symmetry of this electronic configuration. For other configurations, the non-symmetrical electronic distribution and the degeneracy loss of 3d orbitals lead to a stability gain upon coordination, increasing the adsorption energy, as one can see for Ni with a d^8 electronic configuration. These results are in agreement with the ones reported by Karthikeyan *et al.* using a different DFT approach based on the VASP code with the PBE exchange and correlation function.[20]

To determine the most stable coordination site, we plotted the adsorption energy difference between the H and M sites for all 3d TMs, as shown in Fig. 1e. Here, negative values indicate that the M site is the most stable, and positive values mean that H is the most favorable coordination site. As one can see, the H site is the most favorable coordination site for MoS_2–TM, except for Sc and Cu that absorb at the M sites. In addition, for all the MoS_2–TM–Cl_3 complexes, there are only slight energy differences between the H and M sites, with the M site showing slightly higher E_{ads} for all TMs, except for the Sc and Cu. This trend indicates that for all MoS_2–TM–Cl_3 complexes, there are no preferable adsorption sites. For all 3d TMs, the S site was not stable, and the H or M sites showed the highest values of E_{ads}.

Fig. 1f shows the TM's partial charge for MoS_2–TM and MoS_2–TM–Cl_3 complexes analyzed by the Voronoi deformation density method.[21] We notice that TMs with a harder acid character (Sc, Ti, and V) tend to donate more electrons and stabilize with a higher positive charge, meaning that the metal–

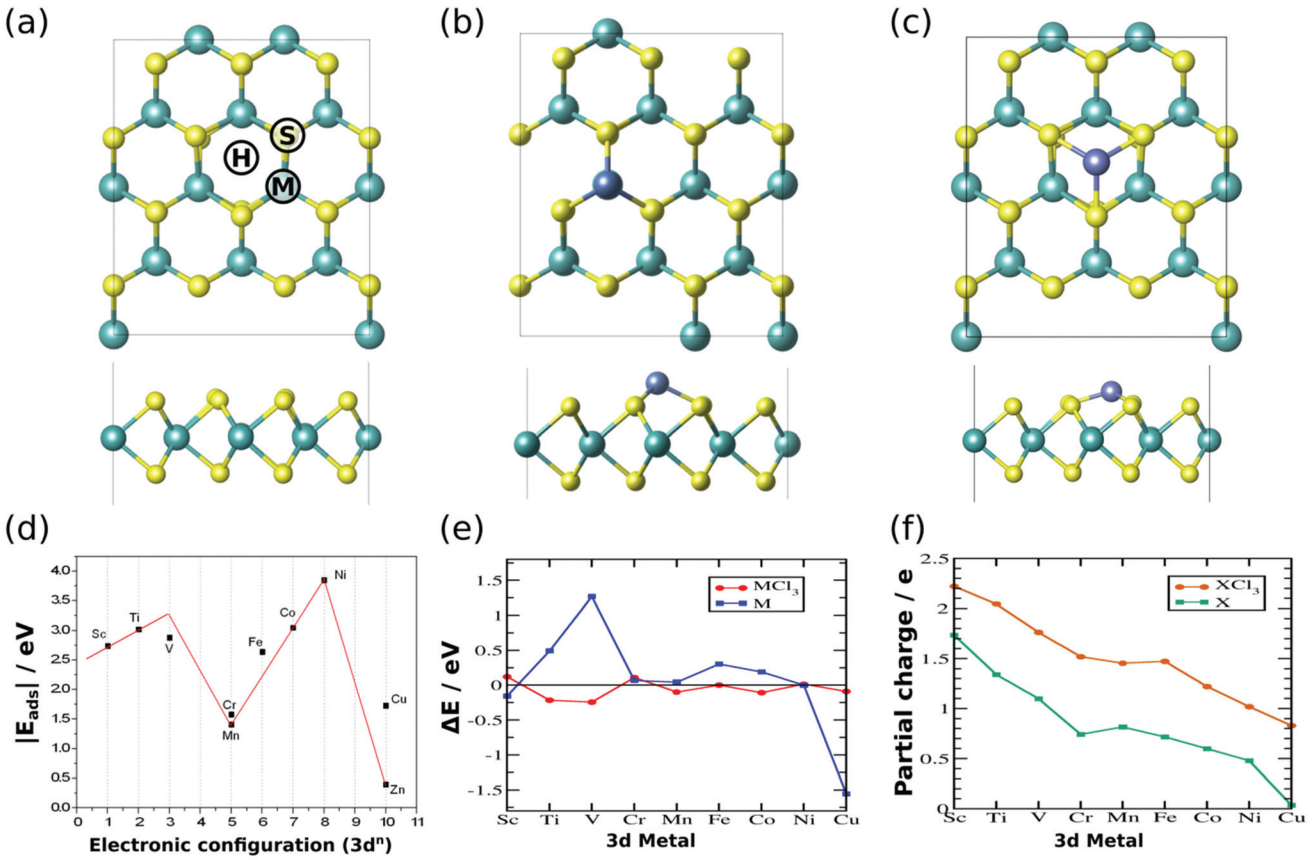

Fig. 1 DFT theoretical analyses of MoS_2–TM complexes. Optimized (relaxed) structures for (a) pristine MoS_2 (possible coordination sites indicated); (b) MoS_2–Co in the M site configuration; and (c) MoS_2–Co in the H site configuration. (d) Adsorption energy as a function of the transition metal electronic configuration for MoS_2–TM complexes. (e) H- and M-site adsorption energy difference for the 3d TMs for MoS_2–TM and MoS_2–TM–Cl_3 coordination compounds. (f) Partial charge for the TMs in the cases of MoS_2–TM and MoS_2–TM–Cl_3 coordination compounds.

sulfur interaction exhibits some ionic nature. This behavior is related to these metals' small ionization energy, leading to a greater tendency to lose the 4s and 3d electrons, leaving the atom with a closed shell and exhibiting higher positive charges. In contrast, for softer metals, such as Co, Ni, and Cu, there is a tendency to form stronger covalent bonds, increase the charge delocalization, and decrease the metal's charge. Since sulfur atoms have a soft base character, the interaction with soft metals leads to a higher adsorption energy due to its more covalent character, as seen by the high E_{ads} for Co and Ni. Furthermore, when the TM's coordination sphere is completed with Cl atoms, the partial charge is higher for all 3d metals.

The electronic band dispersion was calculated to investigate the influence of TM and TM–Cl_3 coordination on the electronic properties of MoS_2. Fig. 2 shows the band dispersion for MoS_2–Co–Cl_3, MoS_2–Ni–Cl_3, and MoS_2–Cu–Cl_3 on both H and M sites, as well as for pristine MoS_2. We notice that for all calculated 3d TMs, the material remained with a direct gap after functionalization. However, the Fermi level energy, the states near the Fermi level, and the spin polarization of these states were drastically affected by the TM's coordinated to the MoS_2 surface (Fig. 2). For example, the adsorption of Co atoms creates new states near the Fermi level, between 0 and 0.5 eV, localized on the Co atoms when the $CoCl_3$ complex is coordinated on the H site (Fig. 2b). On the other hand, when $CoCl_3$ is in the M site (Fig. 2c), new states appear not only near the Fermi level, but also near the conduction band (CB), positioned ~0.25 eV under the CB. MoS_2 → Co charge transfer transitions can lead to new optical absorptions/emissions in the visible and near-infrared spectral ranges. For $NiCl_3$ (Fig. 2c and f), the new levels localized above the Fermi level, at ~0.1 and ~0.75 eV, can lead to MoS_2 → Ni charge transfer transitions, corresponding to optical absorption/emission in the mid and far-infrared regions. The coordination of Cu atoms creates localized states above the Fermi level and near the valence band (VB; Fig. 2d and g) at ~0.05 eV and ~0.5 eV for the Cu coordination at the M and H site, respectively.

For the MoS_2–TM complexes, without Cl atoms, the coordination of a single TM atom leads to new states below the Fermi level, between −1 and 0 eV, for Co and Ni, and for Co, they have different spin polarization, see Fig. S1 in the ESI.† Therefore, the coordination of TM or TM–Cl_3 on the MoS_2 surface can be explored to carefully tune the TMD's optical,

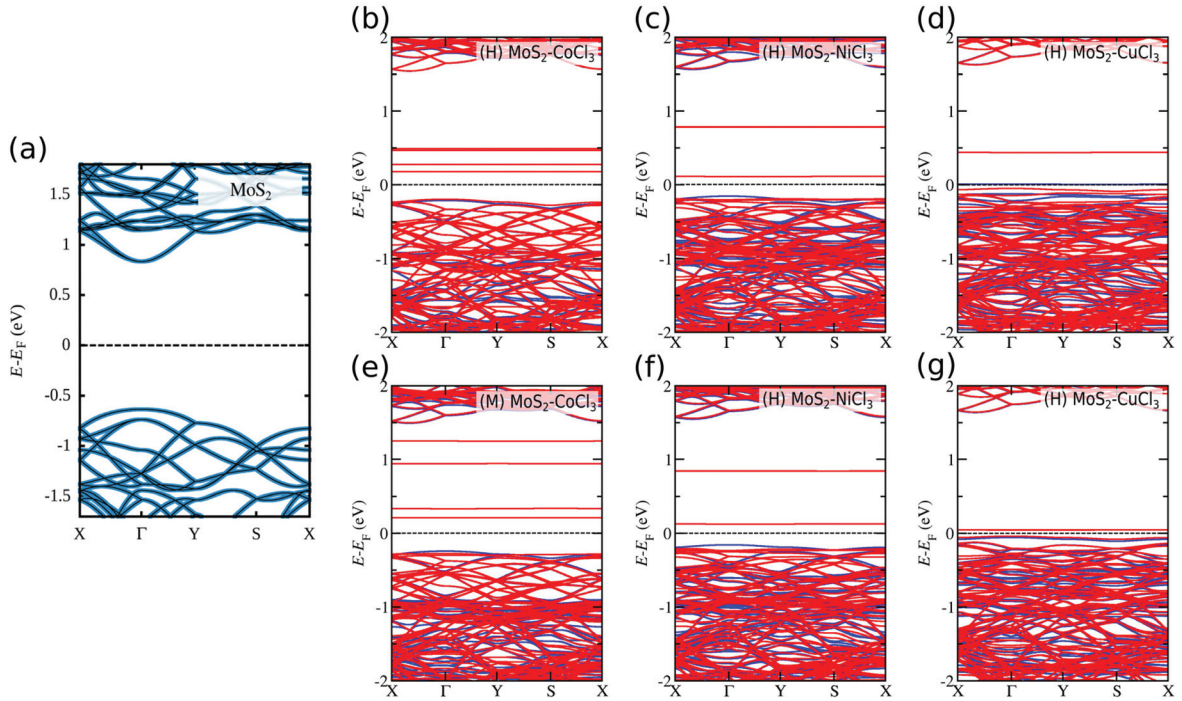

Fig. 2 Electronic band dispersion of TM functionalized MoS_2 calculated by DFT. (a) Electronic structure of pristine MoS_2. (b–g) Electronic band dispersion of Co-, Ni-, and Cu-functionalized MoS_2 *via* H (b–d) and M (e–g) sites with Cl_3 completing the TM's coordination sphere. The blue and red curves indicate states with different spin polarization. The discrete "flat" levels are new states localized on the TM atoms, created after functionalization, suggesting the possibility to control the doping type by means of the TM coordination site. For all systems the Fermi level was shifted to zero.

electronic, and chemical properties by choosing the TM and its coordination sphere. Another important aspect is that these controlled changes can be performed with minimal modifications on the crystalline monolayer since there is no significant change of the Mo–S bond length and Mo–S–Mo bond angle after TM functionalization. This is a clear advantage compared to other doping strategies, such as controlling the vacancy density or interstitial/substitutional doping, where high doping levels cannot be achieved without compromising materials stability and mechanical properties.[22] Based on the DFT calculations, we see that we can perform the functionalization of the MoS_2 monolayer with 3d TMs such as Cr, Mn, Co, Ni, Cu, and Zn. We can now correlate the trends of E_{ads} calculated by DFT with experimental results obtained by photoluminescence, XPS, and REELS, as we shall discuss in the following sections.

Experimental characterization of MoS_2–TM coordination complexes

Doping of MoS_2 *via* TM functionalization. CVD-grown MoS_2 was characterized by Raman spectroscopy and atomic force microscopy. Fig. S2a, in the ESI,† shows the presence of monolayers MoS_2 with an average height of 0.72 nm. The monolayer nature of CVD-grown MoS_2 was also confirmed by Raman spectroscopy where the difference in wavenumber of A_{1g} and E_{2g} is approximately 21 cm^{-1} (Fig. S2b and e†).

TM coordination of MoS_2 was performed by exploring a straightforward acid–base reaction between a Lewis acid, the TM precursor, and a Lewis base, the MoS_2 surface. During the reaction, sulfur's 3p valence electrons are donated to TM's 3d valence orbital, forming an MoS_2–TM coordination bond. The functionalization reactions were performed on CVD-grown MoS_2 monolayers as described in the Methods section. TM chlorides, acetates, and sulfates were chosen since they form labile complexes with TM in aqueous and ethanol solutions, favoring ligand exchange reactions on the TM's coordination sphere. XPS measurements were conducted on MoS_2–TM samples functionalized in a 1×10^{-4} mol L^{-1} TM solution to confirm the presence of TM on the MoS_2 surface. The high-resolution spectra in the specific regions of each TM (Fig. S3†) revealed the presence of the studied metals, and the chemical shift for each one can be related to its chemical environment and the chemical state. Fig. 3 depicts the XPS results and indicates that TM functionalization was effective since we observed shifts on the Mo 3d and S 2p core-levels.

The TM core-level spectra were compared with known species of each TM to elucidate the obtained oxidation states, as shown in Fig. S3.† For Cr, its 2p core-level spectra are comparable to that of Cr_2O_3.[23] Cr 2p orbit exhibits a multiplet splitting with a binding energy of 576.7 eV for Cr^{3+} $2p_{3/2}$ and 586.5 eV for Cr^{3+} $2p_{1/2}$, and a peak separation of 9.8 eV (Fig. S3a†), indicating the presence of Cr^{3+} on the MoS_2 surface. For Mn, the presence of a satellite peak indicates an

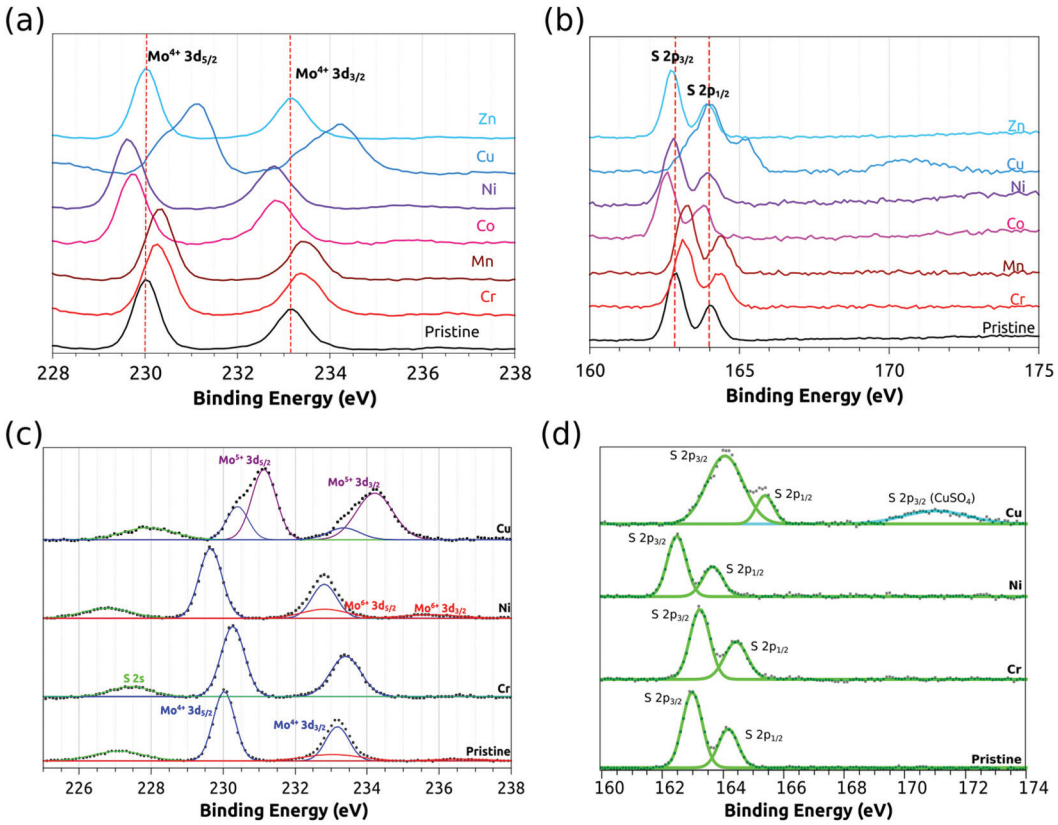

Fig. 3 X-ray photoelectron spectroscopy studies of MoS_2–TM complexes. (a) XPS spectra of Mo 3d orbit on pristine and MoS_2–TM complexes. The curves are the original spectrum after C 1s (284.8 eV) calibration. (b) S 2p orbit of pristine and MoS_2–TM, showing the S $2p_{1/2}$ and $2p_{3/2}$ peaks. (c) Deconvolution of Mo 3d spectra for pristine, MoS_2–Cr, MoS_2–Ni, and MoS_2–TM. The blue curves are the Mo^{4+} $3d_{5/2}$ and $3d_{3/2}$, purple curves are the Mo^{5+} $3d_{5/2}$ and $3d_{3/2}$ peaks, and the red curves are the Mo^{6+} $3d_{5/2}$ and $3d_{3/2}$ peaks. The green curves are the S 2s peak. (d) Deconvolution of S 2p spectra for pristine, MoS_2–Cr, MoS_2–Ni, and MoS_2–TM. The green curves are the S $2p_{1/2}$ and $2p_{3/2}$ peaks, and the blue curve is the S $2p_{3/2}$ for the $CuSO_4$ precursor.

Mn^{2+} oxidation state, and the spectra are comparable to those of MnO, with peaks at 641.2 and 653.2 eV for Mn $2p_{3/2}$ and $2p_{1/2}$, with a slight redshift of 0.2 eV (Fig. S3b†).[23] Co $2p_{3/2}$ 781.1 eV and $2p_{1/2}$ 797.1 eV peaks presented a blueshift of 1.4 eV and are comparable to CoO, with a spin–orbit splitting of 16.0 eV, and characteristic satellites, confirming the presence of Co^{2+} (Fig. S3c†).[23] For Ni, we observed peaks at 856.0 and 873.6 eV, assigned to $2p_{3/2}$ and $2p_{1/2}$, receptively. The Ni 2p core-level spectra are similar to $Ni(OH)_2$, with a prominent blueshift and spin–orbit splitting of 17.6 eV. However, the Ni $2p_{3/2}$ peak seems asymmetric and comparable to NiO, suggesting a mixture of species with the Ni^{2+} state (Fig. S3d†).[23] For Cu, the XPS spectra exhibit a mixture of Cu^{2+} and Cu^{1+}, since there is a satellite peak (938.0 to 947.1 eV) between the Cu $2p_{1/2}$ (952.7 eV) and $2p_{3/2}$ (932.9 eV) peaks; this peak is broad and may have contributions from both Cu^{2+} and Cu^{1+} species (Fig. S3e†).[23] Thus, Cu 2p core-level XPS spectra indicate a reduction of Cu^{2+} to Cu^{1+} during MoS_2 functionalization. Further results suggest that this reduction occurs spontaneously on the MoS_2 surface (see below for details). The Zn spectrum has peaks at 1022.4 and 1045.4 eV, which are assigned to Zn $2p_{3/2}$ and $2p_{1/2}$, indicating a Zn^{2+} oxidation state. This is in good agreement with that of ZnO, showing no shifts (Fig. S3f†).[23]

For all TMs studied here, their oxidation states remained unchanged after functionalization, except for Cu, where the oxidation state reduced. The shifts observed in the MoS_2 XPS spectra can explain the charge transfers between the TM and MoS_2.[24,25] Fig. 3a shows the spectra of the Mo 3d core-level of pristine and doped MoS_2. The deconvolution of the pristine MoS_2 spectrum (Fig. 3c) shows the characteristic Mo^{4+} $3d_{5/2}$ peak at 230.0 eV that we will refer later for further discussion. When MoS_2 is functionalized with a TM, charge transfer may occur, thus leading to new charge densities on Mo and TM atoms; therefore, a shift in the Mo^{4+} $3d_{5/2}$ peak is expected. In this context, a blueshift indicates a charge transfer from Mo to the TM, leading to a more negative character on the TM and a more positive character (p-type doping) on the MoS_2, increasing the binding energy of Mo electrons. Moreover, a redshift indicates a charge transfer from TM to Mo, leading to a more positive TM and a more negative character (n-type doping) in MoS_2, thus decreasing the binding energy of its electrons.

The Mo 3d core-level spectra for the MoS_2–Cu samples indicate the oxidation of Mo^{4+} to higher oxidation states. The

deconvolution of Mo 3d spectra shown in Fig. 3c indicates the presence of Mo^{5+} peaks located at 231.1 and 234.2 eV. Thus, there is spontaneous oxidation of Mo^{4+} to Mo^{5+} followed by the Cu^{2+} to Cu^{1+} reduction, as indicated by the Cu 2p spectra (Fig. S3e†). In Fig. 3c, the deconvolution of Mo 3d spectra of pristine, MoS_2–Cr, and MoS_2–Ni samples are also presented, showing that the oxidation of Mo^{4+} is observed only for the Cu samples. The presence of Mo^{6+} in some pristine and functionalized samples originated from Mo oxide remnants from the CVD synthesis.[26] The S 2p peak in the MoS_2–Cu sample is shifted to higher energies due to the change in the Mo oxidation state; however, it is still in the typical range of sulfides.[23] For all the S spectra (Fig. 3b and d), similar behavior is observed since MoS_2 has a high degree of mixing of Mo and S atomic orbitals.[27]

Bandgap tuning through TM coordination

MoS_2 is a layered semiconductor that shows a transition from indirect to direct bandgap when it reaches a monolayer.[28] To evaluate whether the bandgap remains direct after TM functionalization and study possible shifts on the bandgap values, REELS measurements were performed. Fig. 4 shows the Tauc plot obtained from the REELS spectra, where we can observe that the doping does not change the direct bandgap character, indicated by linear regression on the gap transition presented. All linear regression showed an R^2 of 0.99. Small shifts in the bandgap value can also be observed when analyzing the linear regression and the baseline (Fig. 4). In general, as we can see, TM-functionalization, except Mn and Zn, lowered the bandgap of MoS_2, indicating the creation of new states between the VB and the CB. However, due to the low energy resolution, only the shift observed for Cr and Co samples can be considered. Therefore, experiments with higher resolution are needed to fully understand the influence of TM doping on MoS_2 bandgap values. It is noteworthy that the shoulder between 1.6 and 2.4 eV can be assigned MoS_2 excitons and trions.[29] However, due to our energy resolution, they cannot be separated, and the TM's effects on the excitons will be discussed in the next section based on PL measurements.

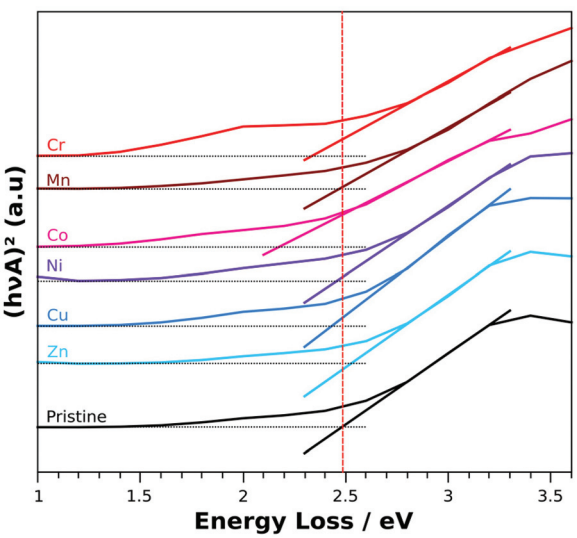

Fig. 4 Tauc-Plot from the REELS data for MoS_2–TM indicated the bandgap by interception between the linear regression and the baseline. All linear regressions presented R^2 = 0.99.

Photoluminescence tuning through TM coordination

Optically generated electron–hole pairs in monolayer MoS_2 form stable exciton states even at room temperature because of the extremely large Coulomb interactions in atomically thin 2D materials.[29,30] The neutral exciton plays an important role in the optical properties of the monolayer. Fig. 5a shows the PL spectra for a typical monolayer with the main excitonic peak at 1.83 eV (exciton A) related to the direct bandgap transition at the K point.[30] PL spectroscopy measurements were carried out for MoS_2–TM complexes at various TM concentrations ranging from 1×10^{-9} mol L^{-1} to 1×10^{-6} mol L^{-1} to study the effect of TM coordination on the optical properties of MoS_2. Fig. 5a shows the PL spectra of pristine and Ni functionalized MoS_2 monolayers. The PL intensity and shape of the A exciton are significantly altered after Ni functionalization and change as a function of TM concentration.

The PL peak can be deconvoluted and fitted by two Lorentzians, the neutral exciton (X) and the trion (X^-), to understand these spectral changes. It can also be seen that the X^- peak was enhanced relative to the X intensity after Ni functionalization. The formation of the coordination π backbonds between the S and Ni atoms results in Ni electrons being transferred to the MoS_2, leading to an increase in the trion intensity relative to the neutral exciton intensity. These changes in exciton and trion populations result in an overall PL quenching and widening due to MoS_2 functionalization, in agreement with the XPS and DFT results mentioned previously.[29] The exact opposite effect is seen for Cu functionalization (Fig. 5e). After Cu functionalization, we note an increase in the exciton intensity relative to the trion intensity, similar to Au functionalization, resulting from p-type doping of MoS_2.[16] Fig. 5(b–d and f–h) further show the exciton to trion ratio for other MoS_2–TM complexes. After TM functionalization, some metal ions such as Cr, Co, and Ni significantly quench the neutral exciton and enhance the trion intensity. For Mn and Zn, we observe only a small quenching effect in the PL, which can be explained by their half shell and full shell 3d configurations.

To further verify the trends in PL spectra as a function of functionalization with different metals, we plotted the normalized exciton to trion ratio percentage change as a function of the 3d metal concentration (Fig. S4†). Similar to that induced by Ni coordination, a high decrease in the exciton–trion ratio was also observed for Cr and Co functionalization. Since the trion has a smaller PL efficiency, the overall PL intensity decreases with Ni, Cr, and Co doping. In contrast, for low concentrations (1×10^{-9} mol L^{-1}–1×10^{-7} mol L^{-1}) of Zn, practically no PL changes were observed. We notice just a small

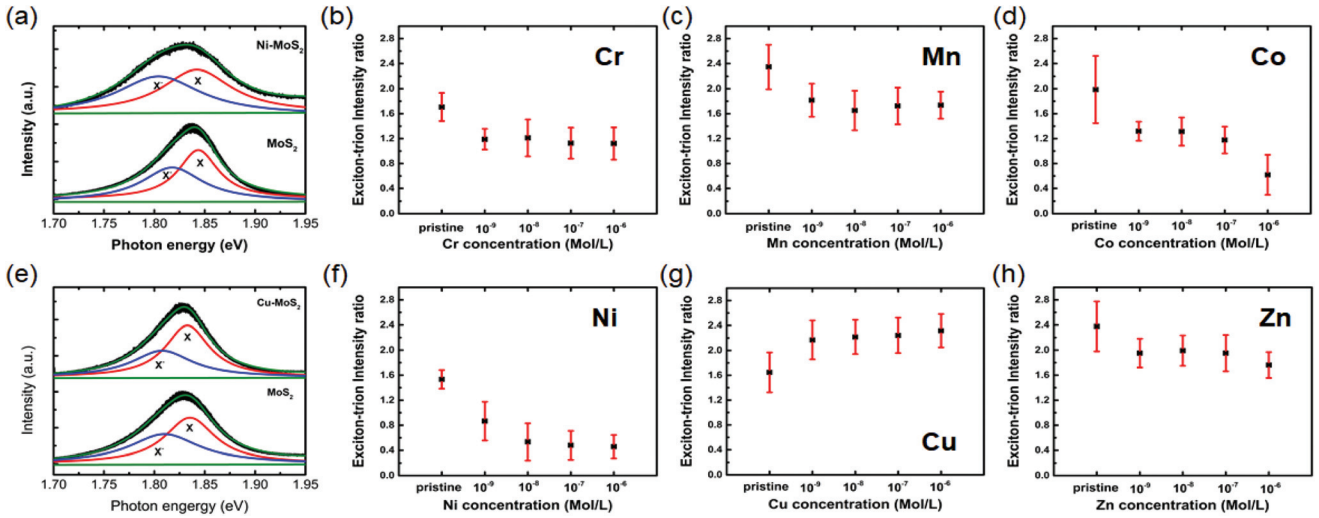

Fig. 5 PL spectral analysis of TM functionalized MoS_2. (a) Photoluminescence spectrum of pristine and functionalized MoS_2 monolayers. The A exciton is deconvoluted into the trion (X-) (blue curve) and exciton (X) (red curve) peaks through Lorentzian functions, also the baseline (green curve). After functionalization, the trion intensity increased while the exciton intensity decreased, which corresponds well with the n-type doping effect of the Ni functionalization. (b) Photoluminescence spectrum of pristine and Cu functionalized MoS_2 monolayers. After functionalization, the trion intensity decreased while the exciton intensity increased, which corresponds well with the p-type doping effect of the Cu functionalization. (b–d and f–h) Exciton to trion intensity ratio of pristine and functionalized MoS_2 for different TM precursors: Cr (b), Mn (c), Co (d), Ni (f), Cu (g), and Zn (h) at different concentrations.

intensity (less than 20% change) decrease for Zn and Mn functionalizations. These results show a remarkable resemblance to the trend of theoretical adsorption energy shown in Fig. 1 and the XPS results. As expected, Mn and Zn showed the smallest effect due to the half and closed-shell configurations, respectively, thus leading to lower stabilization energy for the 3d orbitals upon their coordination with the sulfur atoms on the surface.

In contrast, Ni and Co showed the highest effect on the PL spectra, both in intensity and exciton/trion populations. These results suggest that the effects of Ni coordination on MoS_2 were maximized by the formation of a stronger covalent Ni–S bond, which increases the charge delocalization and the possibility of ligand–metal charge transfers. It is also worth noting that the change in PL shows a positive correlation between the concentration of TM ions in all cases, regardless of n or p doping types.

Morphological characterization

In order to characterize and identify the structure of MoS_2–TM complexes, morphological characterization was performed by optical microscopy, SEM, HAADF-STEM, and STEM simulation. Fig. 6a shows an optical image of the MoS_2–Ni sample where triangular flakes typical of monolayer MoS_2 can be observed. We also notice some multilayer regions with higher contrast and some black points of the MoO_3 residue. Even though we did not observe the formation of TM with zero oxidation state by XPS, SEM was used to evaluate the possible formation of TM-nanoparticles on the MoS_2 surface.[13] Fig. 6b depicts a SEM image of the MoS_2–Ni sample after functionalization with $NiCl_2$ solution at 10^{-4} mol L^{-1}. The MoS_2 monolayer is highlighted in yellow and, as can be seen, even with a high TM concentration, no nanoparticles were present on the flake surface, in agreement with XPS results. High-resolution HAADF-STEM was conducted to study the atomic structure of the TM atoms on MoS_2. The ADF intensity changes depend on the Z-number of atoms ($\sim Z^{1.6-1.9}$),[31] thus, Ni atoms stand out in the MoS_2 lattice. As shown in Fig. 6c, bright single Ni atoms on top of the MoS_2 lattice can be observed, similar to our previously published results on $AuCl_x$ functionalized MoS_2.[16] STEM simulation was performed using Prismatic Software to compare the line scan profiles of MoS_2–Ni. Fig. 6d shows the simulated image, and Fig. 6e and f show the line scan for the experimental and simulated images, respectively. It can be observed that the contrast profile is similar in both cases. The distance between the Ni atoms is similar, 0.978 nm and 1.09 nm for experimental and simulation data. The difference in the intensity ratio between Ni atoms and the regular MoS_2 lattice, 2.16 and 1.46 for experimental and simulation data, can be related to the experimental profile's low signal/noise ratio. Despite the differences, we can clearly see the similarity between the two line scans, confirming the atomic coordination of Ni atoms to the MoS_2 surface. The imaging of other TMs studied, such as Co and Cr, was also performed, but due to their lower Z number and $|E_{ads}|$ compared to Ni, we could not identify these atoms on top of the MoS_2 lattice.

It is noteworthy that the HAADF-STEM image reveals that Ni atoms were found on the MoS_2 basal plane and not on the defect or edge regions, indicating that Ni functionalization occurs by its coordination with the S atoms at the M site, as predicted by DFT calculations. Additionally, experimental and theoretical STEM images prove that TM doping of MoS_2 occurs

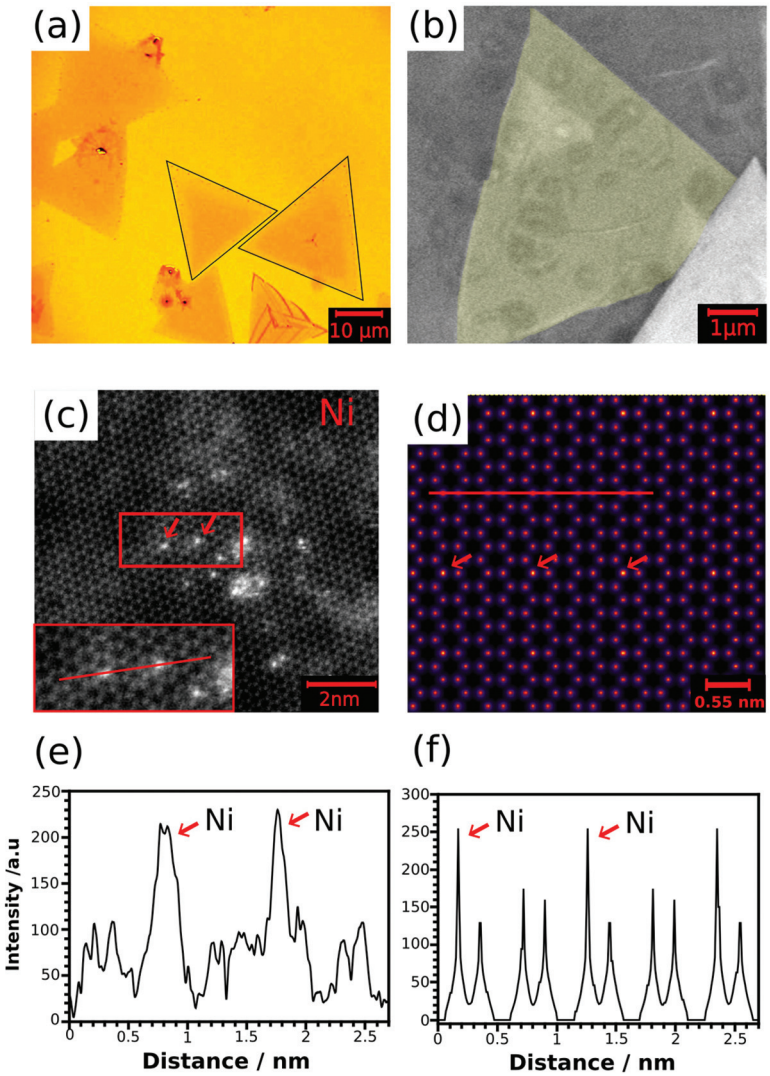

Fig. 6 Imaging of MoS_2 by different microscopy techniques. (a) Optical Microscopy showing triangular MoS_2 monolayer flakes and dark spots of MoO_3. (b) SEM image of a Ni functionalized MoS_2 flake showing the absence of aggregates or Ni nanoparticles. (c) HAADF-STEM image of MoS_2–Ni, where the bright spots show Ni single atoms atomically dispersed on the MoS_2 basal plane, the inset shows where the line profile was acquired. (d) STEM simulation of MoS_2–Ni calculated from the DFT optimized structure. (e) Line scan profile of MoS_2–Ni, the red arrows indicate where the Ni atoms are placed. (f) Line scan profile of the MoS_2–Ni simulation, the red arrows indicate where the Ni atoms are placed.

via coordination on the TMD surface and not *via* the formation substitutional solutions.

To further evaluate TM coordination on the MoS_2 basal plane, PL mapping was performed on pristine and MoS_2–TM samples. The results for a MoS_2–Ni sample functionalized with Ni^{2+} solution at 10^{-7} mol L^{-1} are shown in Fig. S5.† As discussed in the previous sections, Ni functionalized MoS_2 has a decreased exciton/trion ratio and overall PL intensity since the trion has a smaller PL efficiency. Fig. S5† shows that the intensity change is uniform on the whole flake, indicating that Ni coordination is homogeneous on the MoS_2 basal plane. Similarly, we observed a redshift of the PL peak due to the increase in the trion population, which was more pronounced on the flake center. Fig. S6† shows Co functionalization exhibiting a similar behavior, indicating that TM coordination is homogeneous on the entire flake.

Discussion

Recently it was proposed that classical coordination chemistry concepts could be applied to understand the single-atom functionalization of graphene and its derivatives.[11] In our previous work, we expanded this vision to explore the functionalization of MoS_2 with single Au atoms and its effect on a field-effect transistor.[16] Here, coordination chemistry was applied to understand the trends observed for the coordination of 3d-TMs on the MoS_2 surface. The coordination of SA-TM on the 2DM surface can be understood as forming coordination complexes on the material's surface.[11] Thus, an analogy between the molecular orbital theory for coordination complexes and 2DM solid-state physics can elucidate the trends and properties observed after the TM functionalization of MoS_2 mono-

layers. Coordination chemistry and hard–soft acid–base concepts[16,32,33] can lead to a greater understanding and control of the chemical, electrical, and optical properties of 2D materials.

The coordination of individual atoms of transition metals on the MoS_2 monolayer was carried out by exploring ligand exchange reactions in coordination spheres of different transition metal complexes. In these reactions, one or more ligands bound to the metal, chloride or acetate, were replaced by S atoms on MoS_2, creating a covalent bond between the 2D material and the TM without relying on or creating new defects in the material, Fig. 7. MoS_2 can donate electron density to the metal by forming a Sigma bond, using the sulfurs' p electrons in the VB. Simultaneously, the metal can donate electronic density back to MoS_2 through π back-donation involving the metal d orbital and empty states in the MoS_2 CB. Thus, depending on the TM nature, the MoS_2 system will exhibit an n or p-type doping. It is well known that CVD-grown MoS_2 contains a large number of vacancy defects (*e.g.*, S vacancies).[34,35] However, the TM's reactivity around a defect depends on the type of defect and the partial charge it induces in adjacent atoms. For example, if we consider a S vacancy, the TM atoms will likely not go near the vacancy because of the lower electron density.[35] As we demonstrated in our previous work where MoS_2 was doped with single Au atoms, the TM atoms tend to hop from one S site to another without interacting with defects on the MoS_2 basal plane.[16]

Classical Werner coordination complexes with closed-shell (d^{10}) and the half-shell (d^5) TM in a weak-field (low-spin) configuration do not present ligand-field stabilization energy (LFSE) due to the spherical symmetry of these electronic configurations.[36] In contrast, in TMs with d^3 and d^8 electronic configurations, the low-energy ligand orbitals have a higher electron population on low energy orbitals and consequently higher LFSE.[36] Our DFT calculations showed that TM coordination on M and H sites have very close energies when the TM's coordination sphere is complete with Cl ligands. The TM will acquire an octahedral geometry similar to *fac* isomers of TMA_3B_3 complexes in both sites, where 3 S atoms are on one triangular face and the Cl atoms are on the other face. Both S and Cl atoms are π donor ligands; thus, the TM should adopt a weak-field configuration. Since the MoS_2–TM functionalization occurred under mild conditions, we expect that the TM's coordination sphere will be composed of three S atoms and three ligands from the precursor salt, chloride, or acetate in our case. Additionally, we expect that TM coordination on MoS_2 will follow the same trend as that observed for the LFSE shown in Fig. 8a.

The MoS_2–TM complexes with d^{10} (Zn) and d^5 (Mn and Cr) should have smaller adsorption energy (Fig. 1d). For different configurations, the non-symmetrical electron distribution and the degeneracy loss of 3d orbitals lead to a stability gain upon coordination, increasing the adsorption energy. As for classical coordination complexes, Ni, with d^8 electronic configuration, shows higher adsorption energy due to the complete occupancy of the low-energy ligand orbitals.[36] Due to the higher adsorption energy, the MoS_2–Ni complex was the only one stable during e-beam irradiation on HAADF-STEM imaging. Additionally, this higher Eads value leads to a more significant BE shift in the XPS spectra and a more pronounced exciton/trion ratio decrease on MoS_2–Ni samples.

Wissam Saidi calculated the adsorption (E_{ads}) and cohesive (E_{coh}) energies for 3d metals on the MoS_2 surfaces and showed that the E_{ads}/E_{coh} ratio varies between 0.5 and 0.8.[37] Among the 3d TMs, Ni and Co have the largest ratio of $E_{ads}/E_{coh} \approx 0.8$ but are characterized by diffusion barriers of *ca.* 1 eV. Thus, it is expected that these metals could form small clusters following the Stranski–Krastanov growth model. However, in our case, the transition metals were initially adsorbed through the complexes with chlorine, where attractive interactions between functional groups to form clusters are much smaller. In addition, the core-level XPS spectrum reveals that all transition metals coordinated on the MoS_2 surface are cations. Interestingly, the absence of elemental transition atoms should prevent the formation of stable clusters and particles since the coordinated metals are positively charged ions that show electrostatic repulsion. The repulsion and coordination bonding resulted in stable transition metal single ions even at temperatures of 200 °C, as shown in the HAADF-STEM images of annealed samples in Fig. S12.†

To better visualize the observed trends in XPS, REELS, and PL, we plotted the difference between the pristine and MoS_2–TM samples for each experimental parameter analyzed as a function of the number of electrons on d orbitals (n). Fig. 8 compares all trends with the ligand-field stabilization energy for classical coordination complexes. Fig. 8b shows the binding energy shift of Mo and S core levels for MoS_2–TM samples. We can observe a blueshift for Cr, Mn, and Cu,

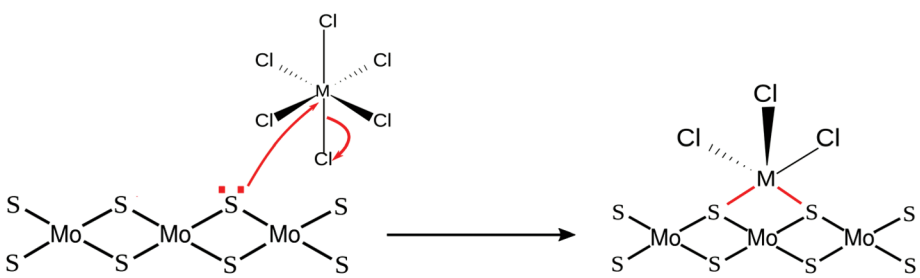

Fig. 7 Reaction scheme for the coordination of transition metals on the MoS_2 surface.

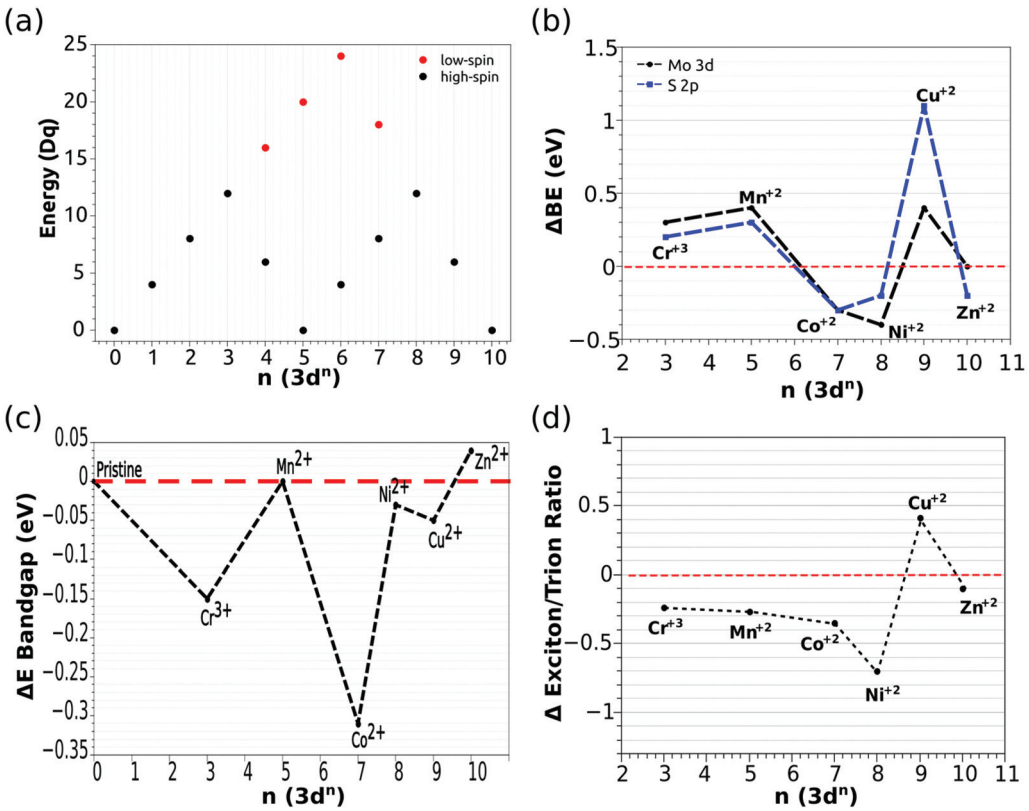

Fig. 8 (a) Ligand-field stabilization energy for 3d TM complexes, showing the weak and strong-field configuration. The ligand-field splitting parameter D_q is equal to $Ze2r^4 = 6a^5$, where Z is the TM charge, e the elementary electron charge, r the TM radius, and the TM–ligand bond distance. (b) Binding energy shift for S $2p_{3/2}$ (blue curve) and Mo $3d_{5/2}$ peak as a function of TM 3d electronic distribution for MoS_2–TM samples. (c) Bandgap shift calculated from the Tauc-plots showed in Fig. 4. (d) Normalized exciton to trion intensity changes showing the percent change in exciton to trion ratio for various TM functionalized MoS_2 samples at different TM concentrations. The TMs here can be separated into three groups. One is Cu, which shows an increase in the exciton to trion ratio, indicating p-type doping on the MoS_2. The second group is Zn, Mn, and Cr, where we see a small decrease in the ratio, indicating weak n-type doping of MoS_2. The last group is Co and Ni, where we see a large decrease in the ratio that corresponds to strong n-type doping of MoS_2.

increasing the binding energy of Mo^{4+} 3d electrons. For Co and Ni, a redshift was observed with ΔBE of −0.3 and −0.4 eV, respectively. For Zn, no considerable shift was observed on Mo 3d peaks. The S 2p core-level spectra indicate the same behavior observed in the Mo 3d spectra for all 3d TM studied here. This is expected since the VB's top and the CB's bottom in MoS_2 show a high degree of mixing of Mo and S atomic orbitals.[27] Therefore, both S and Mo core-level spectra should exhibit similar shifts upon TM coordination. The large shift observed for MoS_2–Ni samples can again be related to Ni^{2+} higher ligand-field stabilization energy.

The Pearson acid–base hard–soft theory can be applied to rationalize the direction of the BE energy shift. When the acid's LUMO level is the closest to the base's HOMO level, the acid–base coordination bond has a more covalent character, and charge transfer may occur between the species' frontier orbitals. When the acid and base valence states have a significant energy difference, the interaction between them has a more ionic character, and some electron withdrawal effects can be observed due to Coulomb interactions. For MoS_2–TM complexes, we can estimate the LUMO of the TM by its electron affinity, and the base's HOMO level is the top of the MoS_2 VB. In order to elucidate the observed trends in XPS spectra of MoS_2–TM samples and how each TM interacts with MoS_2, the energy level diagram shown in Fig. 9 was created using the HOMO and LUMO orbitals of each TM, estimated by the ionization potential and electron affinity of the neutral TM, the TM^{2+}/TM^{1+} redox potentials,[38] and the absolute energies of VB and CB of MoS_2.[39] Although the HOMO and LUMO TM energy levels are referenced to the +1 oxidation state, and the XPS results indicate +2 oxidation states, we expected these energy levels to be lower. However, the same trend is expected, and it is comparable to the experimental data.

Due to the small energy difference between the VB and CB of MoS_2, we can consider it as a soft base (absolute hardness – $\eta \sim 0.9$),[11] which will interact better with a soft acid. The fact that the TM LUMO is relatively close to the MoS_2 VB leads to more covalent bonds and a higher probability of a charge transfer from MoS_2 to the TM. This behavior can be observed for Cr, Mn, Co, and Ni. This leads to the formation of MoS_2–TM coordination complexes with strong Sigma covalent bonds, where S atoms act as a Sigma donor ligand. Mn has an inter-

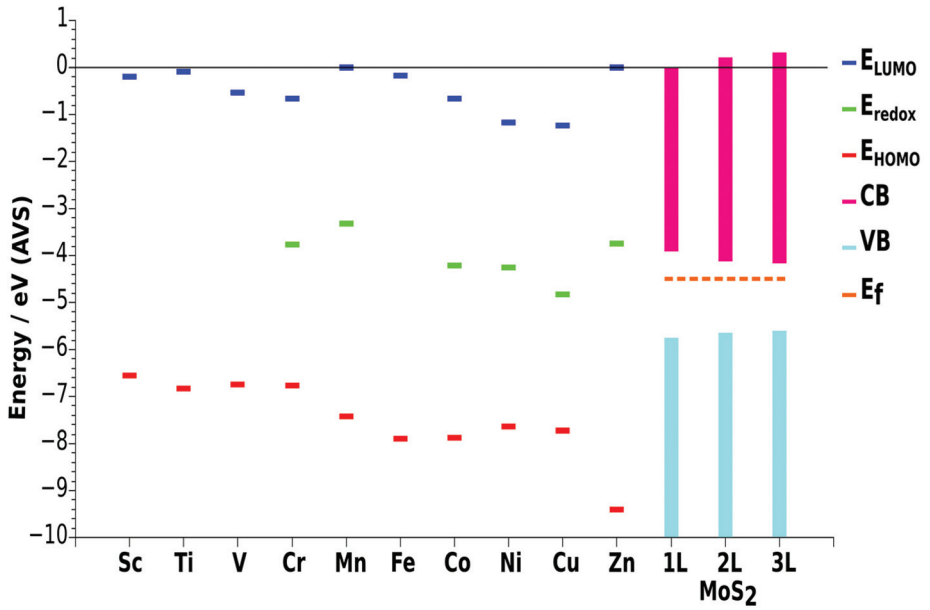

Fig. 9 Diagram of HOMO and LUMO energy of the first-row transition metals and energy values of electronic bands of MoS_2 on the absolute vacuum scale. The red lines indicate HOMO energy of TM, and blue lines indicate LUMO energy of TM, green lines indicate the redox potential of the TM pairs, light blue boxes represent the valence band of MoS_2, pink boxes represent the conduction band of MoS_2, and dot-dashed orange line indicates the Fermi level of MoS_2.

mediary acid character (η = 3.72) and induces a decrease in the electron density of MoS_2, shifting the Mo 3d peaks towards higher energies. Meanwhile, Cr is a softer acid (η = 3.05) and tends to form a more covalent σ bond with S atoms, and the electrons on the MoS_2–Cr bond should be more delocalized. Additionally, S atoms can act as a π donor ligand, thus increasing the charge transfer to the TM and leading to a blueshift in the XPS Mo spectra.

It is noteworthy that Co and Ni show a more donating character. Both are acids with intermediate hardness (η of 3.6 and 3.2, respectively) and tend to form strong covalent bonds with S ligands due to their high ligand-field stabilization energy. Due to their filled 3d orbitals, Co and Ni complexes are known to form π back-bonds with soft ligands.[9] For MoS_2–Ni and MoS_2–Co complexes, there is a σ donation from S to TM and a π back bonding involving the $3d_{xy,\ xz,\ yz}$ TM orbitals and empty orbitals on the MoS_2 CB. The redshift observed on the Mo 3d core-level indicates that the charge transfer from Ni or Co to the MoS_2 is due to the more efficient back-donation. Additionally, this high degree of π back-bonding can increase the trion population, explaining the observed trend in the exciton/trion ratio shown in Fig. 8d. Since Co has smaller E_{ads} than Ni (~1 eV), a higher Co concentration is needed to reach a similar exciton/trion ratio (Fig. S4†).

However, Co and Ni exhibit very different behavior as determined by analyzing the bandgap shift shown in Fig. 8c. MoS_2–Co samples displayed a bandgap shift of approximately 0.3 eV, while MoS_2–Ni samples showed no observable shift. By looking at the electronic band dispersion shown in Fig. 2, we notice that MoS_2–$CoCl_3$ on the M site has a new state localized on Co atoms at ~0.25 eV above the VB. This new state can generate a MoS_2 → Co charge transfer transition with energy close to the bandgap transition. Since our REELS measurements do not have enough resolution to distinguish both transitions, we observed an overall bandgap reduction. For MoS_2–$CoCl_3$ on the H site or for MoS_2–Co (Fig. S1†), there are no new levels near the VB and no new transitions should be observed on the visible region. Thus, the bandgap decrease observed for MoS_2–Co samples could indicate Co coordination on the M site and the presence of Cl on its coordination sphere. For MoS_2–$NiCl_3$ complexes, the DFT calculations indicated the existence of midgap states, and the electronic transition from the VB to these states should occur at around 0.9 eV. This transition is close to the elastic peak on the REELS spectra and cannot be observed, which leads to no changes in the MoS_2 bandgap energy. Optical absorbance measurements conducted on MoS_2 before and after the functionalization with Ni, can provide some information that can be correlated to the band structure. Fig. S10A† depicts the average spectra of 10 pristine (black) and MoS_2–Ni with two Ni concentrations (red – 10^{-8} M and green – 10^{-7} M). There is a small red-shift of the A and B exciton absorption peak, and an increase in the absorption in low photon energies (1.4–1.7 eV) that can be related to new charge transfers transitions between the localized states in the Ni atoms and the MoS_2 levels.

We observe a very low signal in the Cl 2p spectra from the XPS of MoS_2–$NiCl_3$ and MoS_2–$CoCl_3$ (Fig. S7 and S8†). By comparing the peak area of Ni 2p or Co 2p peaks with the Cl 2p peaks as well as considering the relative atomic sensitivity factors (4.5 for Ni, 3.8 for Co, and 0.73 for Cl) of XPS[40] (Tables S2 and S3†), we find that the overall atomic ratios of Ni : Cl and Co : Cl are close to 1 : 3. As discussed earlier, the presence

of Cl anions on the TM coordination sphere could prevent cluster formation. Thus, to investigate the stability of Ni–MoS_2 samples we annealed them at 50, 100, and 200 °C and measured their opto-electronic properties and morphology after the annealing process. Fig. S11† shows the PL spectra of annealed Ni–MoS_2 samples. The samples annealed at 50 °C exhibited PL intensity, exciton/trion ratio (0.4), and FWHM (330 meV) similar to the samples at room temperature, showing that the effect of Ni coordination on MoS_2 remains at temperatures of up to 50 °C. For samples annealed at 100 and 200 °C, the PL intensity, exciton/trion ratios (close to 1.6), and FWHM (280 meV) were similar to the pristine MoS_2. HAADF-STEM images of the annealed samples also indicated that single Ni atoms are still observed for the three temperatures (Fig. S12†). However, some clustering processes can also be observed, suggesting that the effect of a single adatom is lost at a temperature higher than 100 °C due to metal cluster formation.

Zn is the hardest TM in this series (η = 4.72), so there is a poor overlapping between the Zn orbital and MoS_2 orbital, resulting in no variation of the Mo 3d binding energy from the XPS spectra. Additionally, due to the Zn electronic configuration of $3d^{10}$, Zn complexes do not show ligand-field stabilization energy. Hardness and ligand-field stabilization energy both contribute to the Zn's poor interaction with softer ligands. Sulfur atoms in MoS_2 can be considered a soft base, leading to a small BE shift and a slight decrease in the exciton/trion ratio in MoS_2–Zn samples. For these samples, new low energy transitions were not observed in the optical absorbance measurements (Fig. S10†), pointing to a small interaction between MoS_2 and Zn.

For MoS_2–Cu complexes, by comparing the Cu HOMO–LUMO levels with MoS_2 VB–CB energies, we expected a more covalent interaction, albeit with a smaller E_{ads}, as shown in Fig. 7 and 8.[41] However, looking at the TM's redox potential, we notice that Cu has a more negative value, and it is the only one below the MoS_2 Fermi level. Thus, electrons on MoS_2 can be transferred to Cu spontaneously, reducing it from Cu^{2+} to Cu^{1+}. A similar reduction effect was also reported in our previous paper that Au^{3+} could be spontaneously reduced to Au^{1+}. It is noteworthy that we could not discard the possibility of Cu^0 formation; however, we did not observe Cu^0 in the XPS or nanoparticle formation in SEM images. On the other hand, Cu^{1+} does not have ligand-field stabilization energy due to its $3d^{10}$ configuration. However, due to the absence of Jahn–Teller distortions and its softer character, the MoS_2–Cu bond energy should be higher than in Cu^{2+} and Zn^{2+} cases. These electron transfers from MoS_2 to Cu can lower the MoS_2 E_F, explaining the very high BE shift observed on Mo 3d XPS spectra. The high BE shift could also be pointing to the Mo^{4+} oxidation into Mo^{5+}. However, Raman spectra of MoS_2–Cu samples (Fig. S9†) do not show any shift or new peaks when compared to the pristine samples. Therefore, we believe that Cu can induce a high degree of p-type doping on MoS_2, which can be supported by the decrease in the trion population and the increase in the exciton/trion ratio (Fig. 8d).

Conclusions

In this work, we successfully prepared TM–MoS_2 coordination complexes for 3d transition metals (Cr, Mn, Co, Ni, Cu, Zn) and demonstrated that Ni forms single atoms that are bonded to S atoms *via* coordination bonds. This novel approach does not rely on defects or atom substitution and yet implies a significant impact on the optical and electrical properties of the functionalized monolayer MoS_2. The formation of the coordination complexes led to the transfer of electrons between MoS_2 and the transition metal, which can introduce both n- and p-type doping to MoS_2, depending on the transition metal used. Moreover, the degree of n and p-type doping can be fine-tuned by choosing the transition metal and by varying the transition metal precursor concentrations, thus controlling the electronic band structure of MoS_2 and the exciton to trion relative population. In addition, the properties of the TM functionalized MoS_2 display a trend based on the 3d electron configuration of the transition metal that matches the periodic trend of well-studied coordination compounds. This trend can serve as a guide for future chemical functionalization reactions of monolayer TMDs. The synthesis of single atoms introduced in this work could also be exploited in other applications such as single-atom catalysis (SAC), quantum information devices, optoelectronics, and enhanced sensing.

Author contributions

The manuscript was written through contributions of all authors. H. L., W. C. S., and D. G. conducted the functionalization experiments and characterization. L. S. G. S., A. G. V. and M. L. M. R. conducted the XPS and REELS measurements and analysis. L. S. performed first-principles calculations. E. K. and K. T. synthesized the pristine MoS_2 materials. K. F., T. Z. and F. Z. helped with TEM characterization and simulation. Y. L. and Z. Y. provided guidance and helped analyze the data. D. G., M. T., and C. J. S. M. supervised the whole work. All authors gave approval to the final version of the manuscript. H. L. and W. C. S. contributed equally.

Conflicts of interest

There are no conflicts to declare.

Acknowledgements

This work was supported by the São Paulo State Foundation (FAPESP, grant no. 2012/50259-8, 2015/11779-4, 2017/01817-1 and 2018/25339-4), the Brazilian Nanocarbon Institute of Science and Technology (INCT/Nanocarbono), Conselho Nacional de Desenvolvimento Científico e Tecnológico (CNPq), and CAPES – PriInt (Programa Institucional de Internacionalização; Grant no. 88887.310281/2018-00). DG acknowledges financial support from the Rio de Janeiro State

Foundation (FAPERJ – grant no. E-26/010.0022672019 and E-26/211.281/2019) and Serrapilheira Institute (grant number Serra – R-2012-37959). This work was partly supported by the Air Force Office of Scientific Research (AFOSR) through grant No. FA9550-18-1-0072. LS acknowledges financial support from CNPq (Grant No. 408525/2018-5) and high-performance computing facilities from LoboC/NACAD/UFRJ.

References

1 G. R. Bhimanapati, Z. Lin, V. Meunier, Y. Jung, J. Cha, S. Das, D. Xiao, Y. Son, M. S. Strano, V. R. Cooper, L. Liang, S. G. Louie, E. Ringe, W. Zhou, S. S. Kim, R. R. Naik, B. G. Sumpter, H. Terrones, F. Xia, Y. Wang, J. Zhu, D. Akinwande, N. Alem, J. A. Schuller, R. E. Schaak, M. Terrones and J. A. Robinson, Recent Advances in Two-Dimensional Materials beyond Graphene, *ACS Nano*, 2015, **9**(12), 11509–11539, DOI: **10.1021/acsnano.5b05556**.

2 T. Zhang, K. Fujisawa, F. Zhang, M. Liu, M. C. Lucking, R. N. Gontijo, Y. Lei, H. Liu, K. Crust, T. Granzier-Nakajima, H. Terrones, A. L. Elías and M. Terrones, Universal In Situ Substitutional Doping of Transition Metal Dichalcogenides by Liquid-Phase Precursor-Assisted Synthesis, *ACS Nano*, 2020, **14**, 4326–4335, DOI: **10.1021/acsnano.9b09857**.

3 S. Z. Butler, S. M. Hollen, L. Cao, Y. Cui, J. A. Gupta, H. R. Gutiérrez, T. F. Heinz, S. S. Hong, J. Huang, A. F. Ismach, E. Johnston-Halperin, M. Kuno, V. V. Plashnitsa, R. D. Robinson, R. S. Ruoff, S. Salahuddin, J. Shan, L. Shi, M. G. Spencer, M. Terrones, W. Windl and J. E. Goldberger, Progress, Challenges, and Opportunities in Two-Dimensional Materials beyond Graphene, *ACS Nano*, 2013, **7**(4), 2898–2926, DOI: **10.1021/nn400280c**.

4 J. Zheng, K. Lebedev, S. Wu, C. Huang, T. Ayvalı, T.-S. Wu, Y. Li, P.-L. Ho, Y.-L. Soo, A. Kirkland and S. C. E. Tsang, High Loading of Transition Metal Single Atoms on Chalcogenide Catalysts, *J. Am. Chem. Soc.*, 2021, **143**(21), 7979–7990, DOI: **10.1021/jacs.1c01097**.

5 H. Sahin and F. M. Peeters, Adsorption of Alkali, Alkaline-Earth, and 3d Transition Metal Atoms on Silicene, *Phys. Rev. B: Condens. Matter Mater. Phys.*, 2013, **87**, 085423, DOI: **10.1103/PhysRevB.87.085423**.

6 Y. Zhou and E. J. Reed, Structural Phase Stability Control of Monolayer MoTe2 with Adsorbed Atoms and Molecules, *J. Phys. Chem. C*, 2015, **119**, 21674–21680, DOI: **10.1021/acs.jpcc.5b05770**.

7 X. Lin and J. Ni, Much Stronger Binding of Metal Adatoms to Silicene than to Graphene: A First-Principles Study, *Phys. Rev. B: Condens. Matter Mater. Phys.*, 2012, **86**, 075440, DOI: **10.1103/PhysRevB.86.075440**.

8 S. Lei, X. Wang, B. Li, J. Kang, Y. He, A. George, L. Ge, Y. Gong, P. Dong, Z. Jin, G. Brunetto, W. Chen, Z.-T. Lin, R. Baines, D. S. Galvão, J. Lou, E. Barrera, K. Banerjee, R. Vajtai and P. Ajayan, Surface Functionalization of Two-Dimensional Metal Chalcogenides by Lewis Acid–Base Chemistry, *Nat. Nanotechnol.*, 2016, **11**(5), 465–471, DOI: **10.1038/nnano.2015.323**.

9 Y. Ding and Y. Wang, Structural, Electronic, and Magnetic Properties of Adatom Adsorptions on Black and Blue Phosphorene: A First-Principles Study, *J. Phys. Chem. C*, 2015, **119**(19), 10610–10622, DOI: **10.1021/jp5114152**.

10 A. Hashmi and J. Hong, Transition Metal Doped Phosphorene: First-Principles Study, *J. Phys. Chem. C*, 2015, **119**(17), 9198–9204, DOI: **10.1021/jp511574n**.

11 D. Grasseschi, W. C. Silva, R. de Souza Paiva, L. D. Starke and A. S. do Nascimento, Surface Coordination Chemistry of Graphene: Understanding the Coordination of Single Transition Metal Atoms, *Coord. Chem. Rev.*, 2020, **422**((xxxx), 213469, DOI: **10.1016/j.ccr.2020.213469**.

12 R. Gangwar, D. Pandey, S. Kancharlapalli, D. Raychaudhuri, A. Chakrabarti, A. Banerjee and T. K. Ghanty, Ab Initio Study of Adsorption of Fission Gas Atoms Xe and Kr on MoS2Monolayer Functionalized with 3d Transition Metals, *J. Phys. Chem. C*, 2021, **125**(2), 1493–1508, DOI: **10.1021/acs.jpcc.0c08888**.

13 G. Hai, H. Gao, G. Zhao, W. Dong, X. Huang, Y. Li and G. Wang, Difference between Metal-S and Metal-O Bond Orders: A Descriptor of Oxygen Evolution Activity for Isolated Metal Atom-Doped MoS2 Nanosheets, *iScience*, 2019, **20**, 481–488, DOI: **10.1016/j.isci.2019.10.001**.

14 G. Liu, A. W. Robertson, M. M. J. Li, W. C. H. Kuo, M. T. Darby, M. H. Muhieddine, Y. C. Lin, K. Suenaga, M. Stamatakis, J. H. Warner and S. C. E. Tsang, MoS2 Monolayer Catalyst Doped with Isolated Co Atoms for the Hydrodeoxygenation Reaction, *Nat. Chem.*, 2017, **9**(8), 810–816, DOI: **10.1038/NCHEM.2740**.

15 Y. Wang, B. Wang, R. Huang, B. Gao, F. Kong and Q. Zhang, First-Principles Study of Transition-Metal Atoms Adsorption on MoS 2 Monolayer, *Phys. E*, 2014, **63**, 276–282, DOI: **10.1016/j.physe.2014.06.017**.

16 H. Liu, D. Grasseschi, A. Dodda, K. Fujisawa, D. Olson, E. Kahn, F. Zhang, T. Zhang, Y. Lei, R. B. Nogueira Branco, A. L. Elías, R. C. Silva, Y. T. Yeh, C. M. Maroneze, L. Seixas, P. Hopkins, S. Das, C. J. S. de Matos and M. Terrones, Spontaneous Chemical Functionalization via Coordination of Au Single Atoms on Monolayer MoS2, *Sci. Adv.*, 2020, **6**, eabc9308, DOI: **10.1126/sciadv.abc9308**.

17 L. Rangel DaCosta, H. G. Brown, P. M. Pelz, A. Rakowski, N. Barber, P. O'Donovan, P. McBean, L. Jones, J. Ciston, M. C. Scott and C. Ophus, Prismatic 2.0 – Simulation Software for Scanning and High Resolution Transmission Electron Microscopy (STEM and HRTEM), *Micron*, 2021, **151**(August), 103141, DOI: **10.1016/j.micron.2021.103141**.

18 F. A. Cotton, Ligand Field Theory, *J. Chem. Educ.*, 1964, **41**(9), 466, DOI: **10.1021/ed041p466**.

19 H. Irving and R. J. P. Williams, Order of Stability of Metal Complexes, *Nature*, 1948, **162**(4123), 746–747, DOI: **10.1038/162746a0**.

20 J. Karthikeyan, H. P. Komsa, M. Batzill and A. V. Krasheninnikov, Which Transition Metal Atoms Can Be Embedded into Two-Dimensional Molybdenum

Dichalcogenides and Add Magnetism?, *Nano Lett.*, 2019, **19**(7), 4581–4587, DOI: **10.1021/acs.nanolett.9b01555**.

21 C. Fonseca Guerra, J. Handgraaf, E. J. Baerends and F. M. Bickelhaupt, Voronoi Deformation Density (VDD) Charges: Assessment of the Mulliken, Bader, Hirshfeld, Weinhold, and VDD Methods for Charge Analysis, *J. Comput. Chem.*, 2004, **25**(2), 189–210, DOI: **10.1002/jcc.10351**.

22 Z. Lin, B. R. Carvalho, E. Kahn, R. Lv, R. Rao, H. Terrones, M. A. Pimenta and M. Terrones, Defect Engineering of Two-Dimensional Transition Metal Dichalcogenides, *2D Mater.*, 2016, **3**(2), 022002, DOI: **10.1088/2053-1583/3/2/022002**.

23 D. Briggs, X-Ray, Photoelectron Spectroscopy (XPS), in *Handb. Adhes*, 2nd edn, 2005, pp. 621–622. DOI: **10.1002/0470014229.ch22**.

24 Y. Shi, W. M. Huang, J. Li, Y. Zhou, Z. Q. Li, Y. C. Yin and X. H. Xia, Site-Specific Electrodeposition Enables Self-Terminating Growth of Atomically Dispersed Metal Catalysts, *Nat. Commun.*, 2020, **11**(1), 1–9, DOI: **10.1038/s41467-020-18430-8**.

25 Y. Shi, Z. R. Ma, Y. Y. Xiao, Y. C. Yin, W. M. Huang, Z. C. Huang, Y. Z. Zheng, F. Y. Mu, R. Huang, G. Y. Shi, Y. Y. Sun, X. H. Xia and W. Chen, Electronic Metal–Support Interaction Modulates Single-Atom Platinum Catalysis for Hydrogen Evolution Reaction, *Nat. Commun.*, 2021, **12**(1), 1–11, DOI: **10.1038/s41467-021-23306-6**.

26 M. Xiang, H. Liu, C. Huang, Y. Li, H. Zeng and X. Shao, Mo Doping Assisting the CVD Synthesis of Size-Controlled, Uniformly Distributed Single-Layer MoS2on Rutile TiO2 (110), *ACS Appl. Mater. Interfaces*, 2020, **12**(30), 34378–34387, DOI: **10.1021/acsami.0c07997**.

27 T. M. Project, *Materials Data on MoS2 by Materials Project*, 2016. DOI: **10.17188/1202268**.

28 X. Li and H. Zhu, Two-Dimensional MoS2: Properties, Preparation, and Applications, *J. Mater.*, 2015, **1**(1), 33–44, DOI: **10.1016/j.jmat.2015.03.003**.

29 S. Mouri, Y. Miyauchi and K. Matsuda, Tunable Photoluminescence of Monolayer MoS2 via Chemical Doping, *Nano Lett.*, 2013, **13**, 5944–5948, DOI: **10.1021/nl403036h**.

30 A. V. Kolobov and J. Tominaga, *Two-Dimensional Transition-Metal Dichalcogenides*, Springer, 1st edn, 2016, vol. 11. DOI: **10.1039/9781782620112-00001**.

31 P. Hartel, H. Rose and C. Dinges, Conditions and Reasons for Incoherent Imaging in STEM, *Ultramicroscopy*, 1996, **63**(2), 93–114, DOI: **10.1016/0304-3991(96)00020-4**.

32 R. G. Pearson, Hard and Soft Acids and Bases, *J. Am. Chem. Soc.*, 1963, **85**, 3533–3539, DOI: **10.1021/ja00905a001**.

33 R. G. Parr and R. G. Pearson, Absolute Hardness: Companion Parameter to Absolute Electronegativity, *J. Am. Chem. Soc.*, 1983, **105**(26), 7512–7516, DOI: **10.1021/ja00364a005**.

34 Z. Lin, B. R. Carvalho, E. Kahn, R. Lv, R. Rao, H. Terrones, M. A. Pimenta and M. Terrones, Defect Engineering of Two-Dimensional Transition Metal Dichalcogenides, *2D Mater.*, 2016, **3**(2), 022002, DOI: **10.1088/2053-1583/3/2/022002**.

35 V. Carozo, Y. Wang, K. Fujisawa, B. R. Carvalho, A. McCreary, S. Feng, Z. Lin, C. Zhou, N. Perea-López, A. L. Elías, B. Kabius, V. H. Crespi and M. Terrones, Optical Identification of Sulfur Vacancies: Bound Excitons at the Edges of Monolayer Tungsten Disulfide, *Sci. Adv.*, 2017, **3**(4), 1–10, DOI: **10.1126/sciadv.1602813**.

36 D. A. Johnson and P. G. Nelson, Factors Determining the Ligand Field Stabilization Energies of the Hexaaqua 2+ Complexes of the First Transition Series and the Irving-Williams Order, *Inorg. Chem.*, 1995, **34**(22), 5666–5671, DOI: **10.1021/ic00126a041**.

37 W. A. Saidi, Trends in the Adsorption and Growth Morphology of Metals on the MoS2(001) Surface, *Cryst. Growth Des.*, 2015, **15**(7), 3190–3200, DOI: **10.1021/acs.cgd.5b00269**.

38 D. R. Lide, *CRC Handbook of Chemistry and Physics*, 2005. DOI: **10.1201/b17118-9**.

39 K. Keyshar, M. Berg, X. Zhang, R. Vajtai, G. Gupta, C. K. Chan, T. E. Beechem, P. M. Ajayan, A. D. Mohite and T. Ohta, Experimental Determination of the Ionization Energies of MoSe2, WS2, and MoS2 on SiO2 Using Photoemission Electron Microscopy, *ACS Nano*, 2017, **11**(8), 8223–8230, DOI: **10.1021/acsnano.7b03242**.

40 J. F. Moulder, W. F. Stickle, P. E'Sobol and K. D. Bomben, *Handbook of X-Ray Photoelectron Spectroscopy*, Perkin-Elmer Corporation, 1992. DOI: **10.1002/0470014229.ch22**.

41 R. Freitag and J. Conradie, Understanding the Jahn–Teller Effect in Octahedral Transition-Metal Complexes: A Molecular Orbital View of the Mn(β-Diketonato) 3 Complex, *J. Chem. Educ.*, 2013, **90**(12), 1692–1696, DOI: **10.1021/ed400370p**.